Proceedings Paper:
Bidar, O., Anderson, S. and Qin, N. (2024) A priori sensor placement strategy for turbulent mean flow reconstruction using parametric model perturbations. In: AIAA SCITECH 2024 Forum. AIAA SCITECH 2024 Forum, 08-12 Jan 2024, Orlando, FL, USA. American Institute of Aeronautics and Astronautics. Article no: AIAA 2024-1580. ISBN: 9781624107115.

https://doi.org/10.2514/6.2024-1580

A Priori Sensor Placement Strategy for Turbulent Mean Flow Reconstruction Using Parametric Model Perturbations

Omid Bidar*[1], Sean Anderson†[1], and Ning Qin‡[1]

[1]*The University of Sheffield, Western Bank, Sheffield, S10 2TN, UK*

This paper investigates an a priori approach for sparse sensor placement to generate experimental data for turbulent mean flow reconstruction—data assimilation—in the context of steady Reynolds-average Navier-Stokes (RANS) simulations. The strategy utilises perturbations of the turbulent model constants to generate a map of regions in the flow that are most sensitive to the turbulence model. Sensors are targeted at regions of highest sensitivity using a genetic-algorithm optimiser with a minimum distance constraint between any two sensors, to avoid clustering. The data assimilation approach is based on the adjoint-based field inversion, which modifies the transport equation(s) for an existing model with a spatial field, which is then iteratively optimised with the goal of reducing the error between the baseline model output and the high-fidelity data. The separated flow over the periodic hill is used as a test case, with the one-equation Spalart-Allmaras turbulence model. Direct numerical simulation data is used as surrogate experimental data to allow examining the effectiveness of the framework for various scenarios. Preliminary results show that errors in the streamwise velocity predictions can be reduced by over 30% with only five sensors, compared to over 74% reduction when using the data over the entire domain (i.e. data for the $\sim 14.7 \times 10^3$ cells in the mesh).

I. Introduction

In this work we explore an a priori strategy for sparse sensor placement to experimentally generate the data required for turbulent mean flow reconstruction in the context of Reynolds-averaged Navier-Stokes (RANS) solutions. Turbulent flow simulation, utilising the RANS equations, is a widely used computational fluid dynamic (CFD) method for predicting fluid flow in various engineering fields. RANS-based simulations are favoured due to their simplicity and low computational demands, but they often suffer from inaccuracies when dealing with complex flows, due to the modelling of all turbulent scales[1]. The research community has been exploring the combination of RANS solutions with higher-fidelity data obtained from turbulent scale-resolving numerical simulations (e.g., large eddy simulations or direct numerical simulations) and experimental measurements [2]. This approach aims to reconstruct turbulent flow more accurately, thus reducing errors in RANS-based turbulence modelling. Several frameworks have been developed, enabling significant improvements by utilising limited data that can be measured experimentally (e.g. [3–5]). This progress is particularly promising, as generating large and extensive datasets either through experiments or numerical simulations can be prohibitively expensive.

Inaccuracies in RANS-based turbulence modelling can be broadly classified into three categories [2]: parametric (arising from turbulence model constants), functional (stemming from the form of the solved transport equation(s) for turbulence modelling), and structural (resulting from the underlying assumptions used to derive the model, such as the widely employed linear eddy viscosity hypothesis in many popular RANS-based models [6]).

Broadly, turbulent mean flow reconstruction has been investigated in two main streams: ensemble-based, and variational or adjoint-based. In this context, the goal in both streams is to reduce the error in the baseline RANS predictions by solving an inverse problem. Examples of the former include the ensembles-based Kalman filter (EnKF) approach used for turbulent mean flow reconstruction using wall measurements (pressure and skin friction) [7], and a regularised EnKF method using disparate data [4]. While ensemble-based methods minimises a cost function without requiring the derivative of the system states with respect to the control variable, adjoint-based approaches utilise the gradient of the cost function with respect to the system states to search for the optimal solutions. Due to the high-dimensionality of the problem, efficient gradient computations require the adjoint method [8]. Some examples of

*PhD candidate, Dept. of Automatic Control and Systems Engineering, and Dept. of Mechanical Engineering, obidar1@sheffield.ac.uk

†Senior Lecturer, Department of Automatic Control and Systems Engineering

‡Professor, Department of Mechanical Engineering, AIAA Associate Fellow, n.qin@sheffield.ac.uk

adjoint-based flow reconstruction include using velocity profiles [8, 9], wall measurements (skin friction [10], surface pressure [11]), integral data (e.g. lift coefficient [3]), and disparate data (combination of velocity profiles and wall quantities) [5].

Recently, sensor placement has been investigated for ensemble-based data assimilation. Mons *et al.* have investigated unsteady [12] and mean flow reconstruction [13] using the adjoint-based data assimilation, however, they have only investigated this in the context of laminar flows. In the most successful approach [13], they used second-order adjoint solutions to guide sensor placement. While effective, this can be computationally prohibitive for complex three-dimensional turbulent flows of industrial interest. In [14], Deng *et al.* utilise the EnKF approach to perform flow reconstruction by adjusting the model constants. For sensor placement they used a deep neural network which generated the spatial sensitivity of the streamwise velocity field with respect to perturbations in the RANS model constants (i.e. parametric perturbations). This approach has the advantage of being a priori (i.e. data is not required for sensor placement), and is relatively straight-forward to implement. However, flow reconstruction by only adjusting a small number of model constant may not be sufficient to address functional and structural inaccuracies in baseline turbulence models [15].

In the current study, we present a sensor placement strategy that incorporates the parametric perturbations strategy introduced by Deng et al [14]. Additionally, we employ adjoint-based data assimilation techniques to tackle functional uncertainties inherent in the baseline turbulence model, instead of just adjusting model constants. To reconstruct the flow, we adopt a field inversion approach, where the turbulence model's transport equation is modified by introducing a scalar field in each mesh cell. This scalar field is adjusted through a gradient-based optimisation, aiming to achieve a close match with the high-fidelity data. In parallel, we have also pursued another approach based on the eigenspace perturbations of the Reynolds stress tensor to generate the uncertainty map [16].

The remainder of the paper is structured as follows: in Section II we provide an overview of the overall framework, followed by the details of each component. Preliminary results and discussions are provided in Section III, and finally conclusions and planned future work for the final manuscript are outlined in Section IV.

II. Methods

A. Overview

Fig. 1 illustrates an overview of the proposed framework. We start by perturbing the baseline turbulence model constants, in this case the one-equation Spalart-Allmaras turbulence model, and solving the RANS equations. Uncertainty maps for any given quantity (e.g. velocity component, pressure) is generated as a function of the variance for the different perturbations. Given a number of sensors, locations with highest variances are targeted using a genetic algorithm constrained optimisation. Once the optimal sensor locations have been identified, we use the data to perform data assimilation using the field inversion approach.

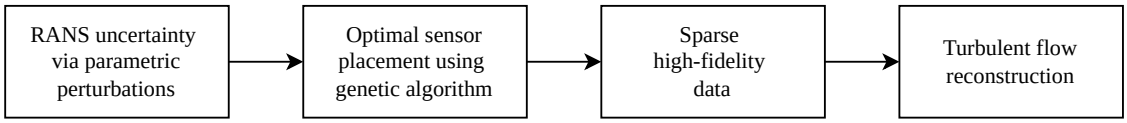

Fig. 1 Overview of the proposed framework.

B. Incompressible RANS

The incompressible steady Navier-Stokes equations are:

$$\int_S \boldsymbol{U} \cdot d\boldsymbol{S} = 0, \tag{1}$$

$$\int_S \boldsymbol{U}\boldsymbol{U} \cdot d\boldsymbol{S} + \int_V \nabla p dV - \int_S (\nu + \nu_t)(\nabla \boldsymbol{U} + \nabla \boldsymbol{U}^T) \cdot d\boldsymbol{S} = 0, \tag{2}$$

where $\boldsymbol{U}$ is the velocity, p is the pressure, ν and ν_t are the molecular and turbulent viscosity, respectively. The RANS equations are solved using the semi-implicit method for pressure linked equations (SIMPLE) algorithm in OpenFOAM.

C. Spalart-Allmaras Baseline Model and Parametric Perturbations

As the turbulence closure, we utilise the popular one-equation Spalart-Allmaras [17] model which defines the turbulent viscosity in Eqn. 2 as a function of the surrogate viscosity $\tilde{\nu}$,

$$\nu_t = \tilde{\nu} f_{v1} \tag{3}$$

where the transport equation for $\tilde{\nu}$ is:

$$\int_V \nabla \cdot (\boldsymbol{U}\tilde{\nu}) dV - \underbrace{C_{b1} \int_V \tilde{\Omega}\tilde{\nu} dV}_{\text{production}} - \underbrace{\frac{1}{\sigma} \int_V \nabla \cdot [(\nu + \tilde{\nu})\nabla\tilde{\nu}] + C_{b2}|\nabla\tilde{\nu}|^2 dV}_{\text{transport}} + \underbrace{C_{w1} \int_V f_w \left(\frac{\tilde{\nu}}{d}\right)^2 dV}_{\text{dissipation}} = 0, \tag{4}$$

with the following intermediate functions

$$\begin{aligned} f_{v1} &= \frac{\chi^3}{\chi^3 + C_{v1}^3}, \qquad \chi = \frac{\tilde{\nu}}{\nu}, \qquad f_w = g\left[\frac{1 + C_{w3}^6}{g^6 + C_{w3}^6}\right]^{1/6}, \qquad g = r + C_{w2}(r^6 - r), \\ r &= \frac{\tilde{\nu}}{\tilde{\Omega}\kappa^2 d^2}, \qquad \tilde{\Omega} = \Omega + \frac{\tilde{\nu}}{\kappa^2 d^2} f_{v2}, \qquad f_{v2} = 1 - \frac{\chi}{1 + \chi f_{v1}}, \qquad C_{w1} = \frac{C_{b1}}{\kappa^2} + \frac{1 + C_{b2}}{\sigma}, \end{aligned} \tag{5}$$

where $\tilde{\Omega}$ is the strain rate tensor, $\kappa = 0.41, \sigma = 2/3, Cb1, C_{b2}, C_{w2}, C_{w3}$ and C_{v1} are model coefficients. The S-A specific model constants are:

$$C_{b1} = 0.1355, \quad C_{b2} = 0.622, \quad C_{w2} = 0.3, \quad C_{w3} = 2.0, \quad \text{and} \quad C_{v1} = 7.1. \tag{6}$$

Following Deng *et al.* in [14], we vary the constants between 50-150% of their original values. Perturbations include perturbing each constant separately, as well as, perturbing all constants simultaneously, with the bounds for each constant outlined below:

$$\begin{aligned} 0.0678 \leq C_{b1} \leq 0.2033, \\ 0.311 \leq C_{b2} \leq 0.933, \\ 0.15 \leq C_{w2} \leq 0.45, \\ 1.0 \leq C_{w3} \leq 3.0, \\ 3.55 \leq C_{v1} \leq 10.65. \end{aligned} \tag{7}$$

D. Sensor placement using a genetic algorithm optimiser

Each parametric perturbation described in the previous subsection results in a corresponding CFD prediction of all system states, i.e. velocity, pressure, and turbulent viscosity. To generate the uncertainty map, i.e. regions of flow most sensitive to parametric perturbations to target for sensor placement, we calculate the variance of any quantity, Q, from all the perturbed solutions.

Upon the calculation of the uncertainty map, optimal sensor locations are sought by solving a gradient-free optimisation with a cost function of the following form:

$$\begin{aligned} \min_{\boldsymbol{x}} \quad & \left[\sum_{i=1}^{N_S} variance(Q)_{\boldsymbol{x},i}\right]^{-1}, \\ \text{subject to} \quad & d_S \geq d_{\min}, \end{aligned} \tag{8}$$

where N_S is the total number of sensors to be placed, $\boldsymbol{x} \in \Omega$ is a vector of the optimal sensor coordinates to be found, with Ω as the region encompassing all potential sensor positions. The constraint is essential as it is imposed to avoid the clustering of sensors in one region with highest variance. Thus, the minimum distance between any two sensors, d_S, must be greater than or equal to a minimum distance specified by the user $d_{\min}$, defined as a percentage of the characteristic length of the geometry.

E. Turbulent flow reconstruction through field inversion

For turbulent mean flow reconstruction we use the adjoint-based field inversion method. In order to conduct field inversion, a multiplicative scalar field is introduced into the production term of the transport equation in an existing turbulence model. For the one-equation Spalart-Allmaras model the general form of the model's transport equation (Eqn. II.C) for the surrogate variable, represented as $\tilde{\nu}$, is then modified as follows:

$$\int_V \nabla \cdot (\boldsymbol{U}\tilde{\nu}) dV - \beta(\boldsymbol{x})\,\mathcal{P}(\tilde{\nu}, \boldsymbol{w}) - \mathcal{T}(\tilde{\nu}, \boldsymbol{w}) + \mathcal{D}(\tilde{\nu}, \boldsymbol{w}) = 0, \tag{9}$$

where $\mathcal{P}$, $\mathcal{T}$, and $\mathcal{D}$ are the production, transport, and dissipation terms of the transport equation respectively, and are functions of the surrogate viscosity variable $\tilde{\nu}$ and $\boldsymbol{w}$, which represents all the Reynolds-averaged conserved flow variables. $\beta(\boldsymbol{x}, t) \in \mathbb{R}^{n_\beta}$ with n_β representing the number of mesh cells, is the corrective field, and $\beta = 1$ everywhere in the mesh recovers the baseline model.

To minimise the functional error in the baseline turbulence model, we seek to determine the optimum discrepancy field by minimising the difference between high-fidelity data, denoted as $\boldsymbol{d} \in \mathbb{R}^{N_d}$ (where N_d represents the number of data points), and the RANS output, denoted as $\mathcal{G}(\beta)$. This minimisation process involves optimising an objective function of the following form:

$$\min_{\beta} \quad \mathcal{J} = \|\mathcal{G}(\beta) - \boldsymbol{d}\|_2^2 + \lambda \|\beta - \beta_{\text{prior}}\|_2^2, \tag{10}$$

where $\|\cdot\|_2$ represents the L_2 norm. The parameter λ serves as a relaxation or regularisation parameter, while β_{prior} is usually assumed to be 1. This assumption biases the solution towards the baseline model and helps prevent an ill-posed optimisation problem.

Due to the high-dimensional nature of the optimisation problem, gradient-free approaches are computationally infeasible, and thus a gradient-based approach is preferred. Yet still, to compute the gradients efficiently, the adjoint method should be utilised. For this we employ our open-source tool previously introduced in [8].

III. Results and Discussions

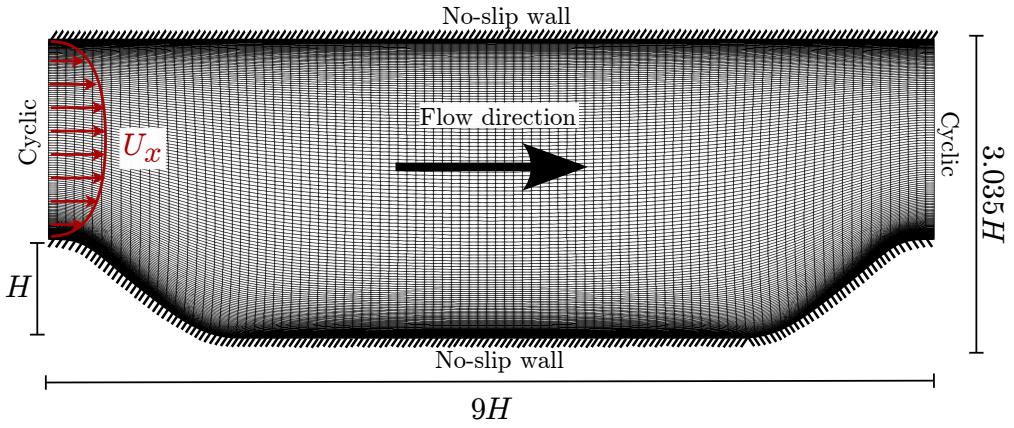

Fig. 2 The structured mesh for the periodic hill, along with the normalised dimensions, and the boundary conditions.

The periodic hill case, depicted in Fig. 2, is used as a test case for the proposed framework. As the flow progresses over the initial hill, it experiences separation, resulting in a large recirculating bubble surrounded by an unsteady shear layer. Subsequently, reattachment occurs, followed by intense acceleration at the subsequent hill. The flow along the top wall remains attached with high pressure gradients. These complex characteristics pose challenges for accurate predictions using RANS turbulence models, hence the popularing of the periodic hill as a benchmark case. We use the direct numerical simulation data by Xiao *et al.* [18]. The Reynolds number based on the bulk velocity is 5600. To maintain a constant bulk velocity a source/forcing term is incorporated into the x-momentum equation (Eqn. 2) as follows:

$$Re_b = \frac{U_b H}{\nu}, \qquad U_b = \frac{1}{2.035H} \int_H^{3.035H} U_x\,(y)\,dy, \tag{11}$$

where U_b is the bulk velocity, ν is the kinematic viscosity, and U_x is the streamwise velocity component.

Fig. 3 shows key results from the parametric perturbations. The velocity profiles clearly show discrepancy between the baseline S-A predictions, and the DNS data. In particular, the baseline model struggles to capture the flow near the walls, especially, in the separated shear layer next to the initial wall. These are also reflected in the perturbation results, where the maximum bounds for the streamwise velocity profiles (Fig. 3 (a)) are in the near wall regions.

The uncertainty maps—variance of the predicted quantities following parametric perturbations—show very different regions of uncertainty depending on which quantity is being illustrated, Figs. 3 (c-f). The key map is for the streamwise velocity, as the velocity components are commonly measured experimental quantities. We focus on the streamwise velocity as it is the dominant component, and henceforth, use it for sensor placement, and subsequently, turbulent mean flow reconstruction.

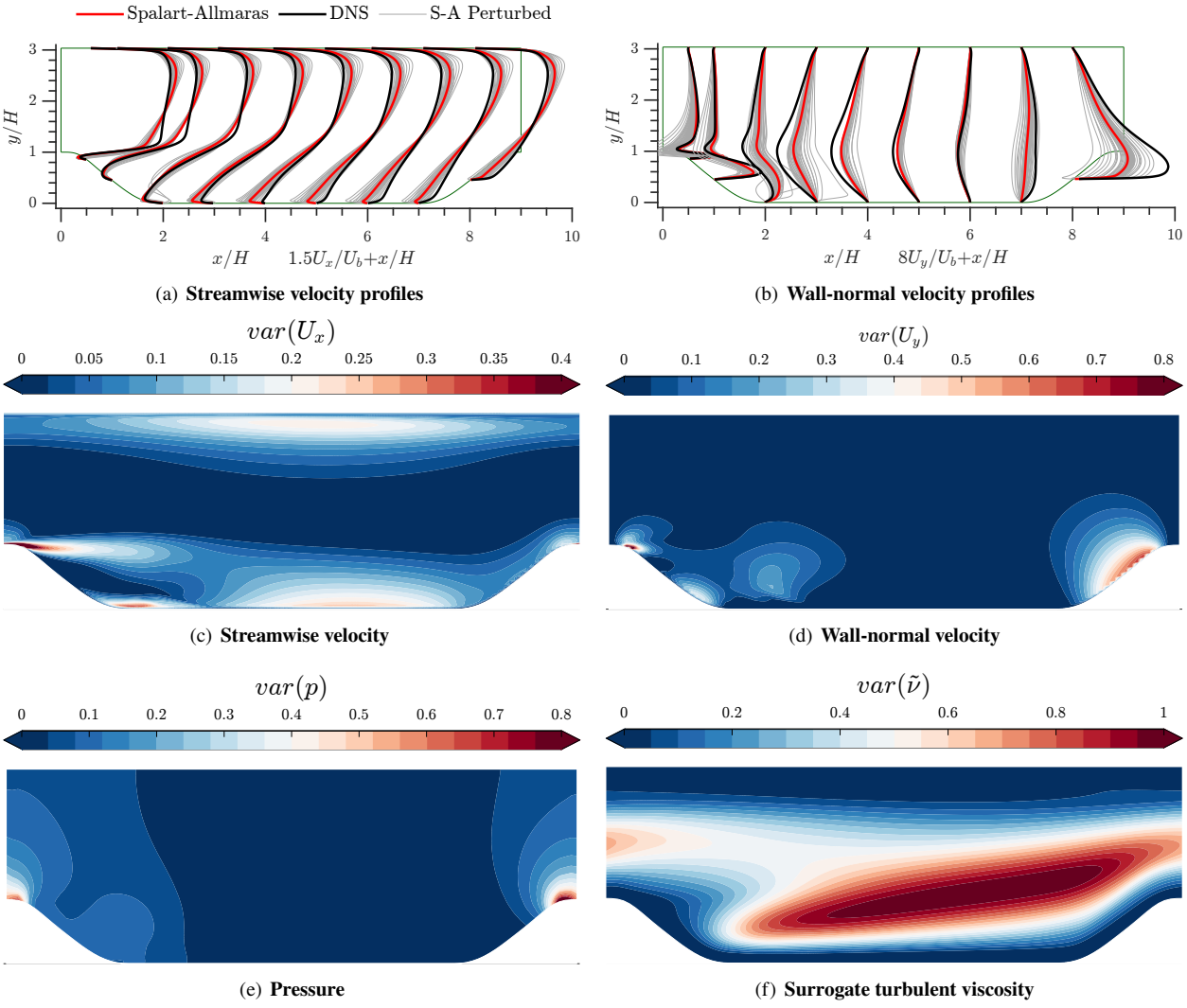

(a) **Streamwise velocity profiles**

(b) **Wall-normal velocity profiles**

(c) **Streamwise velocity**

(d) **Wall-normal velocity**

(e) **Pressure**

(f) **Surrogate turbulent viscosity**

Fig. 3 Uncertainty maps for various quantities, and velocity profiles.

In these preliminary results, we start with five sensors. The optimal locations from the genetic algorithm optimisation is shown in Fig. 4. The minimum distance constraint (as described in Section II.D) is half of the hill height, H. While the optimiser targets generally regions of high uncertainty, as desired, some regions, e.g. the separation bubble close to initial hill, is missed. This will be further explored for the final paper.

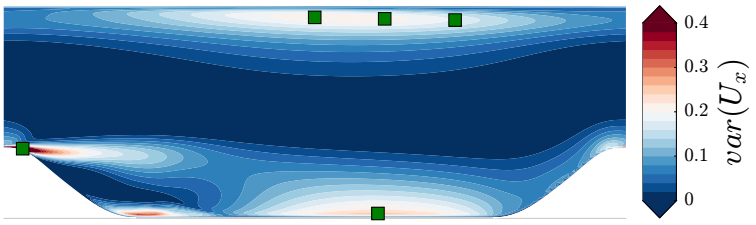

Fig. 4 Optimal sensor locations for five sensors illustrated by the green squares.

The main reconstructed flow results are shown in Fig. 5. The streamwise velocity profiles are better matched to the DNS predictions in the regions near the walls. However, there are some discrepancies towards the centre of the domain, which is identified the least susceptible to parametric perturbations (Fig. 3 (c)). This means that this approach of identifying regions of uncertainty may only be partially adequate. Nevertheless, it is still possible to achieve considerable error reductions in the flow predictions with only 5 sensors, as also highlighted in the wall-normal velocity profiles in Fig. 5 (b), and the skin friction predictions in Fig. 6.

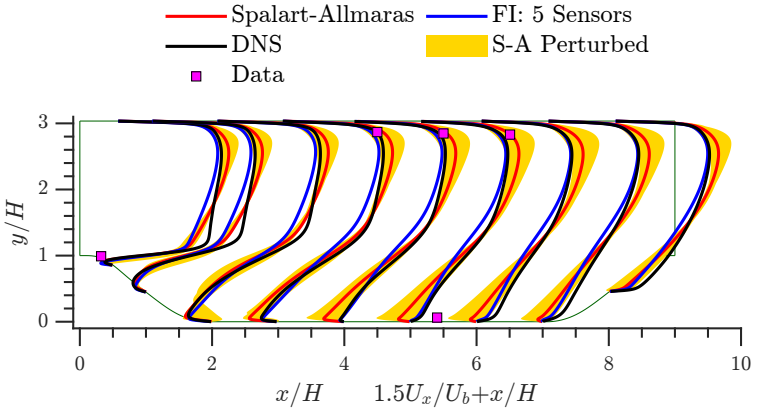

(a) **Streamwise velocity**

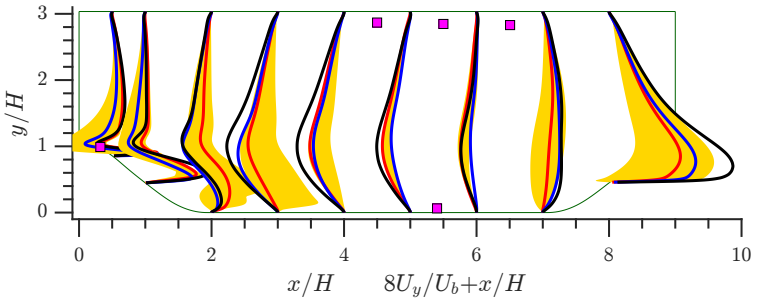

(b) **Wall-normal velocity**

Fig. 5 Comparison of the velocity profiles components after data assimilation with just 5 U_x data points.

Table 1 Comparison of root-mean-squared error reduction.

Scenario	RMSE U_x	% reduction	RMSE U_y	% reduction
Baseline Spalart-Allmaras	0.0027	-	0.0007	-
Field inversion: 5 sensors	0.0019	30.15	0.0005	20.34
Field inversion: entire U_x field	0.0007	74.37	0.0002	66.74

The root-mean-squared error comparison in Table 1 shows that data assimilation with just 5 sensors can reduce the error

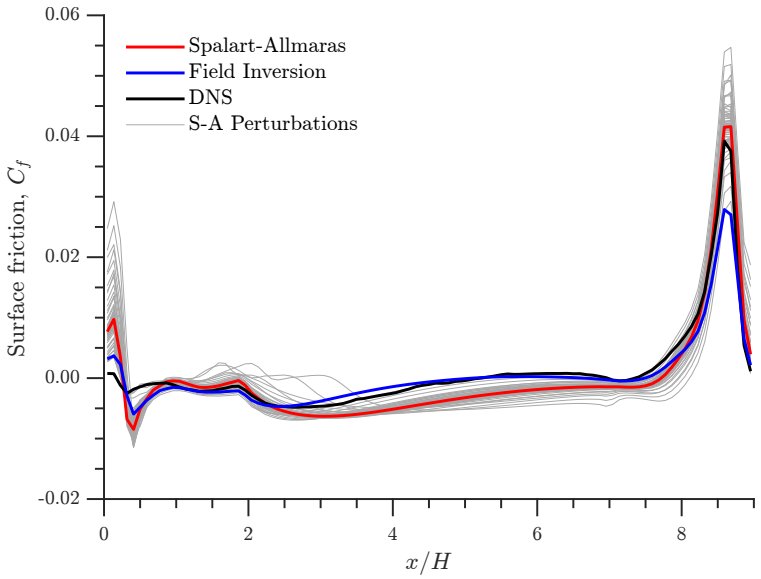

Fig. 6 Comparison of skin friction predictions on the lower wall. Field inversion results only used 5 data points.

in corresponding data used by over 30%, compare to over 74% reduction when using the data for the entire domain. The streamwise velocity contours for the scenarios shown in the table are also illustrated in Fig. 7 (b). There are considerable discrepancies in the baseline predictions, which are significantly reduced with field inversion. Fig. 7 (a) shows the corrective field modifying the baseline equation to reconstruct the flow. It is clear that this is a very complex, highly non-linear, correction where the production of turbulent viscosity is generally magnified near the walls.

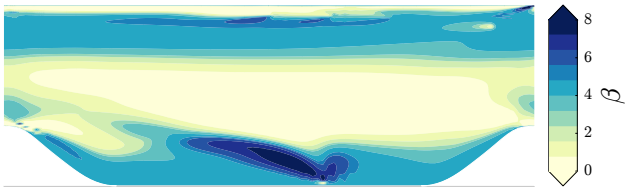

(a) **Corrective field for field inversion with 5 sensors.**

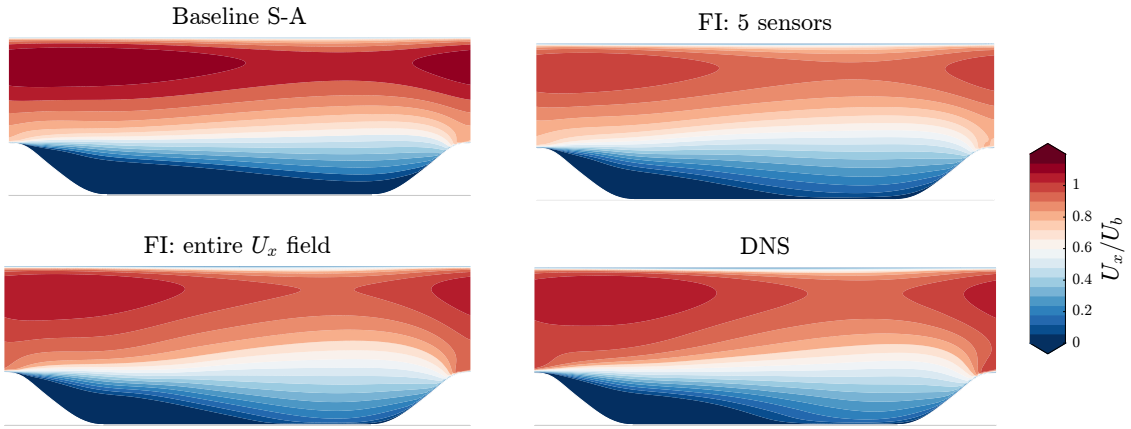

(b) **Normalised streamwise velocity fields.**

Fig. 7 Corrective field modifying the surrogate viscosity and a comparison of the streamwise velocity fields for different scenarios.

IV. Conclusion and future work

We introduced a sensor placement strategy which allows data assimilation for turbulent mean flow reconstruction with sparse data. One of the key advantages of this approach is its a priori nature, i.e. no experimental measurements are needed when deciding sensor locations. Instead, we rely on perturbing the model constants for an existing turbulence model, Spalart-Allmaras in this case, and using it to generate a spatial uncertainty map highlighting regions of flow most sensitive to the perturbations. These regions are then targeted for sensor placement through an optimiser—genetic algorithms in this work. Initial results on a typical benchmark case—the periodic hill—which is poorly predicted by the baseline turbulence model, demonstrate encouraging results where substantial error reduction is achieved with only five sensors/data points. However, there are two key parameters in the optimisation process when placing the sensors which will be investigated in the future: 1) number of sensors, 2) minimum distance between sensors. The latter is required to ensure that sensors are not clustered in just one region of uncertainty.

Acknowledgement

Omid Bidar's work is funded by the University of Sheffield Engineering and Physical Sciences Research Council (EPSRC) Doctoral Training Partnership Scholarship.

References

[1] Durbin, P. A., "Some Recent Developments in Turbulence Closure Modeling," *Annual Review of Fluid Mechanics*, Vol. 50, No. 1, 2018, pp. 77–103. https://doi.org/10.1146/annurev-fluid-122316-045020.

[2] Duraisamy, K., Iaccarino, G., and Xiao, H., "Turbulence Modeling in the Age of Data," *Annual Review of Fluid Mechanics*, Vol. 51, No. 1, 2019, pp. 357–377. https://doi.org/10.1146/annurev-fluid-010518-040547.

[3] Singh, A. P., Medida, S., and Duraisamy, K., "Machine-Learning-Augmented Predictive Modeling of Turbulent Separated Flows over Airfoils," *AIAA Journal*, Vol. 55, No. 7, 2017, pp. 2215–2227. https://doi.org/10.2514/1.j055595.

[4] Zhang, X.-L., Xiao, H., He, G.-W., and Wang, S.-Z., "Assimilation of disparate data for enhanced reconstruction of turbulent mean flows," *Computers & Fluids*, Vol. 224, 2021, p. 104962. https://doi.org/10.1016/j.compfluid.2021.104962.

[5] Bidar, O., He, P., Anderson, S., and Qin, N., "Turbulent Mean Flow Reconstruction Based on Sparse Multi-sensor Data and Adjoint-based Field Inversion," *AIAA AVIATION 2022 Forum*, American Institute of Aeronautics and Astronautics, 2022. https://doi.org/10.2514/6.2022-3900.

[6] Launder, B. E., and Sandham, N. D. (eds.), *Closure Strategies for Turbulent and Transitional Flows*, Cambridge University Press, 2001. https://doi.org/10.1017/cbo9780511755385.

[7] Colburn, C. H., Cessna, J. B., and Bewley, T. R., "State estimation in wall-bounded flow systems. Part 3. The ensemble Kalman filter," *Journal of Fluid Mechanics*, Vol. 682, 2011, pp. 289–303. https://doi.org/10.1017/jfm.2011.222.

[8] Bidar, O., He, P., Anderson, S., and Qin, N., "An Open-Source Adjoint-based Field Inversion Tool for Data-driven RANS modelling," *AIAA AVIATION 2022 Forum*, American Institute of Aeronautics and Astronautics, 2022. https://doi.org/10.2514/6.2022-4125.

[9] Parish, E. J., and Duraisamy, K., "A paradigm for data-driven predictive modeling using field inversion and machine learning," *Journal of Computational Physics*, Vol. 305, 2016, pp. 758–774. https://doi.org/10.1016/j.jcp.2015.11.012.

[10] Duraisamy, K., Singh, A.-P., and Pan, S., "Augmentation of Turbulence Models Using Field Inversion and Machine Learning," *55th AIAA Aerospace Sciences Meeting*, American Institute of Aeronautics and Astronautics, 2017. https://doi.org/10.2514/6.2017-0993.

[11] Belligoli, Z., Dwight, R. P., and Eitelberg, G., "Reconstruction of Turbulent Flows at High Reynolds Numbers Using Data Assimilation Techniques," *AIAA Journal*, Vol. 59, No. 3, 2021, pp. 855–867. https://doi.org/10.2514/1.j059474.

[12] Mons, V., Chassaing, J.-C., and Sagaut, P., "Optimal sensor placement for variational data assimilation of unsteady flows past a rotationally oscillating cylinder," *Journal of Fluid Mechanics*, Vol. 823, 2017, pp. 230–277. https://doi.org/10.1017/jfm.2017.313.

[13] Mons, V., and Marquet, O., "Linear and nonlinear sensor placement strategies for mean-flow reconstruction via data assimilation," *Journal of Fluid Mechanics*, Vol. 923, 2021. https://doi.org/10.1017/jfm.2021.488.

[14] Deng, Z., He, C., and Liu, Y., "Deep neural network-based strategy for optimal sensor placement in data assimilation of turbulent flow," *Physics of Fluids*, Vol. 33, No. 2, 2021, p. 025119. https://doi.org/10.1063/5.0035230.

[15] Xiao, H., and Cinnella, P., "Quantification of model uncertainty in RANS simulations: A review," *Progress in Aerospace Sciences*, Vol. 108, 2019, pp. 1–31. https://doi.org/10.1016/j.paerosci.2018.10.001.

[16] Bidar, O., Anderson, S., and Qin, N., "Sensor placement for data assimilation of turbulence models using eigenspace perturbations," , 2023, pre-print.

[17] Spalart, P., and Allmaras, S., "A one-equation turbulence model for aerodynamic flows," *30th Aerospace Sciences Meeting and Exhibit*, American Institute of Aeronautics and Astronautics, 1992. https://doi.org/10.2514/6.1992-439.

[18] Xiao, H., Wu, J.-L., Laizet, S., and Duan, L., "Flows over periodic hills of parameterized geometries: A dataset for data-driven turbulence modeling from direct simulations," *Computers & Fluids*, Vol. 200, 2020, p. 104431. https://doi.org/10.1016/j.compfluid.2020.104431.